
Comparing information content of representation spaces for disentanglement with VAE ensembles

Kieran A. Murphy Sam Dillavou Dani S. Bassett

University of Pennsylvania

{kieranm, dsb}@seas.upenn.edu dillavou@sas.upenn.edu

Abstract

Disentanglement is the endeavour to use machine learning to divide information about a dataset into meaningful fragments. In practice these fragments are representation (sub)spaces, often the set of channels in the latent space of a variational autoencoder (VAE). Assessments of disentanglement predominantly employ metrics that are coarse-grained at the model level, but this approach can obscure much about the process of information fragmentation. Here we propose to study the learned channels in aggregate, as the fragments of information learned by an ensemble of repeat training runs. Additionally, we depart from prior work where measures of similarity between individual subspaces neglected the nature of data embeddings as probability distributions. Instead, we view representation subspaces as communication channels that perform a soft clustering of the data; consequently, we generalize two classic information-theoretic measures of similarity between clustering assignments to compare representation spaces. We develop a lightweight method of estimation based on fingerprinting representation subspaces by their ability to distinguish dataset samples, allowing us to identify, analyze, and leverage meaningful structure in ensembles of VAEs trained on synthetic and natural datasets. Using this fully unsupervised pipeline we identify “hotspots” in the space of information fragments: groups of nearly identical representation subspaces that appear repeatedly in an ensemble of VAEs, particularly as regularization is increased. Finally, we leverage the proposed methodology to achieve ensemble learning with VAEs, boosting the information content of a set of weak learners—a capability not possible with previous methods of assessing channel similarity.

1 Introduction

The goal of disentanglement is to break information into useful pieces. What qualifies as useful depends on the context: although statistical independence between the pieces of information is the predominant desideratum [1], interpretability of the factors can be prioritized [2] and will clash with independence when correlations are present [3]. Other useful properties proposed for disentanglement are compositionality under group operations [4, 5] and performance enhancement on downstream tasks [6].

A significant challenge in disentanglement research is evaluation. Studies generally evaluate models against ground truth factors of variation on synthetic datasets [7–10]. However, it has been found that repeat trials for models with identical hyperparameters produce significant variation [1], introducing model selection as an additional obstacle to the ultimate goal of fully unsupervised disentanglement. Methods of unsupervised model selection have been proposed based on model centrality [11, 12]: models that are more related to others are presumed disentangled. Yet, relatedness has failed to account for the nature of the models as channels of information transmission. Instead, probabilistic representations are reduced to points by either sampling or taking the means of posterior distributions.

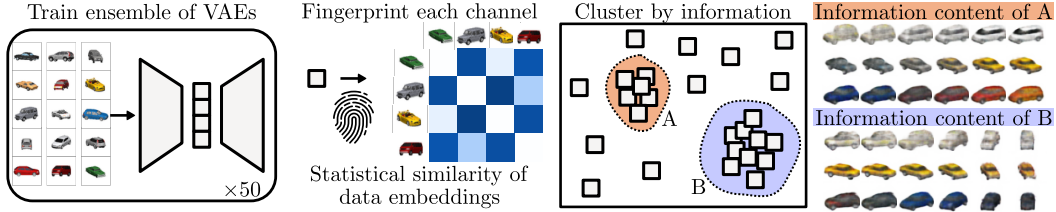


Figure 1: **Discovering structure in ensembles of learned channels.** Given an ensemble of VAE-based models trained on a particular dataset, we take each latent dimension as a channel communicating certain information about the data. A lightweight fingerprint of a channel’s information content can be taken with the pairwise similarity of a sample of data embeddings. We then compare the fingerprints of channels by extending two classic methods to compare clusterings, and look for dense regions where particular pieces of information are repeatedly found throughout the ensemble. In this example, two dense groups are found, labeled A and B, whose information content can be visualized by performing latent traversals across elements in the group.

Then representation spaces are compared by correlation or linear regression [11], methods that are blind to an infinite variety of invertible transformations that preserve information.

In this work, we treat representation spaces as channels for information transmission, and specifically as performing a soft clustering of the data. We extend classic information-theoretic measures of similarity between clusterings to be applicable to probabilistic representation spaces. By comparing the information content of learned representation spaces produced by many models in an ensemble, we are able to identify specific bits of information that are found repeatedly. The focus naturally shifts from identifying central models to identifying central pieces of information. With this new view of how models fragment information about data, we gain a deeper understanding of the various inductive biases engineered to make the disentanglement problem practical [1].

Our primary contributions are the following:

1. We generalize two classic measures that compare the information content of clusterings for the comparison of probabilistic representation spaces.
2. We propose a lightweight method to assess information content based on fingerprinting each representation space with the distinguishability of a sample from the dataset (Fig. 1).
3. The fingerprint itself can be optimized via gradient descent; we demonstrate how to achieve ensemble learning with the representation spaces from many weak VAEs.

2 Related work

The proposed method builds upon classic means of comparing different cluster assignments (clusterings) of a dataset, extending them to compare the information content of probabilistic representation spaces. The method is then used for an empirical approach to unsupervised disentanglement, where the pieces of information consistently found by repeat runs of a model are identified.

2.1 Similarity of clusterings, similarity of representation spaces

The capacity to compare transformations of data produced by different machine learning models enables ensemble learning, a deeper understanding of methodology, and benchmarking [13]. Strehl and Ghosh [14] used outputs of clustering algorithms to perform ensemble learning, based on a measure of similarity between clustering assignments that we will extend in this work: the normalized mutual information (NMI). Referred to as consensus clustering or ensemble clustering, combining multiple clustering outputs can leverage any of a variety of similarity measures [15–19]. Another measure backed by information theory is the variation of information (VI), coined by Meilă [20] for clusters but recognized as a metric distance between information sources at least twice before [21, 22].

Commonly referred to simply as ‘clustering’, *hard* clusterings assign every input datum to one and only one output cluster and have been generalized to multiple forms of *soft* clustering [23]. We focus specifically on *fuzzy* clustering, where membership is assigned by degree to multiple clusters and

must sum to one for each datum [24–26]. We adopt the perspective of probabilistic representation spaces as assigning each input datum to a continuum of clusters—represented by the support in the latent space—with degree of membership expressed by the posterior distributions. To compare soft clusterings is less straightforward than comparing hard clusterings: Extensions for fuzzy clusters have been proposed for measures that only indirectly assess information by counting agreement of assignments, such as the Rand index [13, 27–30]. Information-based measures have been extended for specific types of soft clusters [31, 23] but none, to our awareness, for comparing the information content of fuzzy clusterings over a continuum of clusters.

A rich area of research compares deterministic representation spaces via the pairwise geometric similarity of a common set of data points in the space [32–34], building upon representational similarity analysis from neuroscience [35]. We incorporate the same idea into our approach for comparing probabilistic representation spaces, though with statistical similarity of a set of datapoints instead (Fig. 1), which enables efficient estimation of information theoretic quantities.

2.2 Unsupervised disentanglement

Disentanglement is the problem of splitting information into useful pieces, possibly for interpretability, compositionality, or stronger representations for downstream tasks. Shown to be impossible in the fully unsupervised case [1, 36], research has moved to investigate how to utilize weak supervision [36–39] and incorporate inductive biases [5, 7, 40–42].

A significant challenge for disentanglement is evaluation and model selection when no ground truth is available. When a dataset’s generative factors are available for evaluation, models are compared against an idealized disentanglement where the factors are whole and separate in latent dimensions, [7, 8], and possibly simply encoded [9, 10]. However, there can be significant variation in such metrics across random initializations of the same method and model [1], necessitating unsupervised routes to model selection. Duan et al. [11] proposed that disentangled models are more similar to each other than are entangled ones, in an ensemble of repeats. They evaluated the similarity between two models with an *ad hoc* function of dimension-wise similarity, which was computed as the rank correlation or the weights of a linear model between embeddings in different one-dimensional spaces. ModelCentrality [12] is similar: the model most central in an ensemble is taken to be the most disentangled, with similarity quantified with the FactorVAE score [8], where one model’s embeddings serve as the labels for another model. PIPE [43] is an unsupervised disentanglement metric that relies on a characterization of the posterior distributions in a single model rather than an ensemble. In this work we shift focus from assessing model similarity to channel similarity, under the premise that the fragmentation of information at the core of disentanglement is more naturally studied via the information fragments themselves.

3 Method

At its core, the proposed method compares the information transmitted about a dataset by different representation spaces. We extend two classic measures of similarity between hard clusterings to be applicable to probabilistic representation spaces, which can be understood as performing soft clustering of data. The measures are composed of mutual information terms that can become impractical when evaluating the pairwise comparison of many spaces, so we develop a lightweight estimation method built upon fingerprinting spaces with matrices of pairwise statistical similarities of a sample set of data points.

Our focus in this work is on variational autoencoders (VAEs) [44], a class of generative models that learn a probabilistic latent space that enables regularization in terms of the information transmitted through the space. Let the random variable X represent a sample $x \sim p(x)$ from the dataset under study. X is transformed by a stochastic encoder parameterized by a neural network to a variable $U = f(X, \epsilon)$, where ϵ is the source of stochasticity. We will make use of two fundamental quantities in information theory [45], the entropy of a random variable $H(Z) = \mathbb{E}_{z \sim p(z)}[-\log p(z)]$ and the mutual information between two random variables $I(Y; Z) = H(Y) + H(Z) - H(Y, Z)$. The encoder maps each datapoint x to a posterior distribution in the latent space, $p(u|x)$, and the information passed into U about X is regularized by a variational upper bound [46], the expected Kullback-Leibler (KL) divergence [45] between the posterior distributions and an arbitrary prior $r(u)$: $I(X; U) \leq \mathbb{E}_{x \sim p(x)}[D_{\text{KL}}(p(u|x)||r(u))]$. Commonly, the posteriors and the prior are set to be normal distributions, where the analytic form for the KL divergence is known.

3.1 Comparing representation (sub)spaces as soft clusterings

Consider a clustering of data as communicating certain information about the data. By observing the cluster assignment U instead of a sample X from the dataset (example in Fig. 2a), information $I(X; U)$ will have been conveyed. For a *hard* clustering, where every data point is assigned unambiguously to a cluster (Fig. 2b), the information is equal to the entropy of the clustering, $H(U)$. Given two clusterings U and V , how should their information content be compared?

We focus on two classic measures to compare clusterings. The first is the normalized mutual information (NMI) [14],

$$\text{NMI}(U, V) = \frac{I(U; V)}{\sqrt{H(U)H(V)}} = \frac{H(U) + H(V) - H(U, V)}{\sqrt{H(U)H(V)}}, \quad (1)$$

and the second is the variation of information (VI) [20],

$$\text{VI}(U, V) = H(U|V) + H(V|U) = 2H(U, V) - H(U) - H(V). \quad (2)$$

Both NMI and VI can be straightforwardly applied to hard clusterings. Here however we adopt the perspective of probabilistic representation spaces as *soft* clusterings: instead of merging data points such that they are indistinguishable within a given hard cluster, probabilistic representation spaces offer a continuously varying distinguishability between data points based on overlap between their posterior distributions. The support in latent space can be seen as a continuum of fuzzy clusters [24, 26], one at each at location u , and a datapoint x is assigned membership according to its posterior $p(u|x)$ (Fig. 2c,d).

We extend the two methods of comparing hard clusterings by recognizing that the communicated information, $I(U; X)$, is a natural replacement for the entropy of the hard cluster $H(U)$, that maintains a consistent interpretation for hard and soft clusters. Namely, we replace each entropy term with the mutual information with regards to the data X : $\text{NMI}(U, V) = (I(X; U) + I(X; V) - I(X; U, V)) / \sqrt{I(X; U)I(X; V)}$ and $\text{VI}(U, V) = 2I(X; U, V) - I(X; U) - I(X; V)$. In this form NMI and VI are unchanged for hard clusters, but can now be applied to soft clusters.

However, an important subtlety arises when these metrics are used to compare identical soft clusterings. For probabilistic representation spaces learned by a VAE, or indeed any stochastic communication channel, the stochasticity is external from the design of the channel. Two channels U and U' with identical design have equivalent single message information $I(X; U) = I(X; U')$, but the information contained in their combination may be greater than either individually, $I(X; U, U') \geq I(X; U)$, because the stochasticity is sampled twice. As a result, between identical channels U and U' the proposed extension to $\text{NMI}(U, U')$ could be less than one, and similarly $\text{VI}(U, U')$ could be greater than zero. We account for the information contained in a repeated measurement, which we denote $I(X; U, U')$. NMI requires correction in the normalization constant, and becomes

$$\text{NMI}(U, V) = \frac{I(X; U) + I(X; V) - I(X; U, V)}{\sqrt{(2I(X; U) - I(X; U, U'))(2I(X; V) - I(X; V, V'))}}. \quad (3)$$

VI is corrected by subtracting the average of the self-distances of the two channels, and becomes

$$\text{VI}(U, V) = 2I(X; U, V) - I(X; U, U') - I(X; V, V'). \quad (4)$$

When comparing hard clusterings, $I(X; U, U')=I(X; U)=H(U)$; NMI and VI remain unchanged.

3.2 Efficient estimation by distinguishability fingerprint

We seek an efficient way to capture the information content of a channel for downstream comparison. To this end, we use the pairwise distinguishability of a sample set of data, communicated by the channel, to represent the information. We will leverage a crucial advantage for probabilistic representation spaces: we have access to posterior distributions for each data point, which facilitates the computation of statistical similarity between pairs of datapoints.

To assess statistical similarity between posteriors $p(u|x_1)$ and $p(u|x_2)$ in a given channel, we employ the Bhattacharyya coefficient [47, 48], $\text{BC}(p, q) = \int_{\mathcal{Z}} \sqrt{p(z)q(z)} dz$, which has several desirable properties. First, the BC between two normal distributions (of arbitrary dimensionality) is analytic and can be computed in bulk via efficient array operations. Second, once a matrix $\text{BC}_{ij} :=$

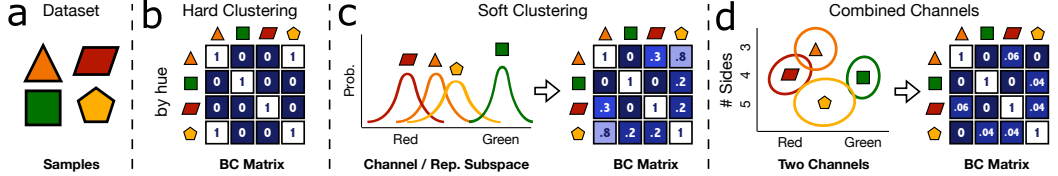


Figure 2: **Channels as conveying partial distinctions and performing soft clustering.** (a) Simple example dataset. (b) Bhattacharyya matrices for hard clusterings (by hue), in which all elements are 0 or 1. (c) Noisy measurements (channels) result in partial distinguishability (soft clustering), and thus matrix elements between 0 and 1. (d) Combining two channels results in superior distinguishability. The Bhattacharyya matrix may be calculated from the measurements, or directly from the matrices of individual measurements.

$BC(p(u|x_i), p(u|x_j))$ of the pairwise values for a random sample of N datapoints is obtained, a lower bound for the information transmitted by the channel can be estimated with the following, from Kolchinsky and Tracey [49], $I(X; U) \geq \frac{1}{N} \sum_i \log \frac{1}{N} \sum_j BC_{ij}$ (under mild assumptions discussed in Appx. C). Third, hard clustering is naturally represented as a distinguishability matrix with entries that are either zero or one. For fast estimation of the information content of a learned channel with respect to a particular generative factor, we can treat the label information for the data sample as arising from a hard clustering according to that factor. Finally, the distinguishability matrix BC_{ij} for the combination of channels U_1 and U_2 is their elementwise product. In other words, receiving both of the messages from channels U_1 and U_2 leads to a distinguishability between data points, as computed by the Bhattacharyya coefficient, that is simply the product of the distinguishability under U_1 and that under U_2 separately. Together, the properties allow the Bhattacharyya matrices to be computed quickly, once for each channel and then saved. Then all subsequent clustering analysis can be done with only the matrices—*i.e.*, without having to load the models into memory again.

We experimentally verify that the BC distinguishability matrices can be used for information estimation (Fig. 3). With 500 channels randomly sampled from β -VAEs trained on the `dsprites` dataset by the authors of Locatello et al. [1], we compare estimates for the information transmitted by each channel $I(X; U)$ to the bounds in Poole et al. [50] using 10,000 data points. We additionally compare the time of computation—loading the saved model, encoding the examples, and computing the estimate for $I(X; U)$. While the time per estimate is roughly comparable (30-40 milliseconds) for the largest distinguishability matrix and for that of Poole et al. [50], greater than $10\times$ speed up comes with only minor performance drop for the size 300 and 100 distinguishability matrices. For computation of the combination mutual information terms $I(X; U, V)$ necessary for NMI and VI, the advantage is greater: elementwise multiplication adds negligible time for our method, and nearly doubles the time for information estimation via Poole et al. [50] to 50msec per estimate. We note that a benefit of focusing on the information of individual channels is that they transmit small amounts (often less than 10 bits) of information, which require fewer samples to reliably estimate.

3.3 Discovering hot spots among learned channels

Our motivating premise is that structure might exist in the learned channels of an ensemble of models. Given the proposed information-theoretic distances between channels—the negative log NMI or the raw VI—we use density-based clustering to search for groups of channels that are found repeatedly across training runs. OPTICS [51] is a clustering method that orders elements in a set by traversing through the set according to proximity. It produces a “reachability” profile—similar to a dendrogram produced by hierarchical clustering but more comprehensible for large sets of points [52]—where valleys indicate denser regions and thus natural groupings of the set of points. For each ensemble, we visualize structure via the reachability profile, the reordered pairwise similarity matrix—NMI or the exponentiated negative VI—which will show a block diagonal form in the case of dense groupings, and the NMI with ground truth labels provided with the dataset.

3.4 Ensemble learning

Consider a set of similar channels found by an ensemble of weak learners. In the spirit of “knowledge reuse” [14] originally applied to ensembles of hard clusters, we might obtain a superior channel from the synthesis of the channels in the set. In contrast to assessments of representation space similarity

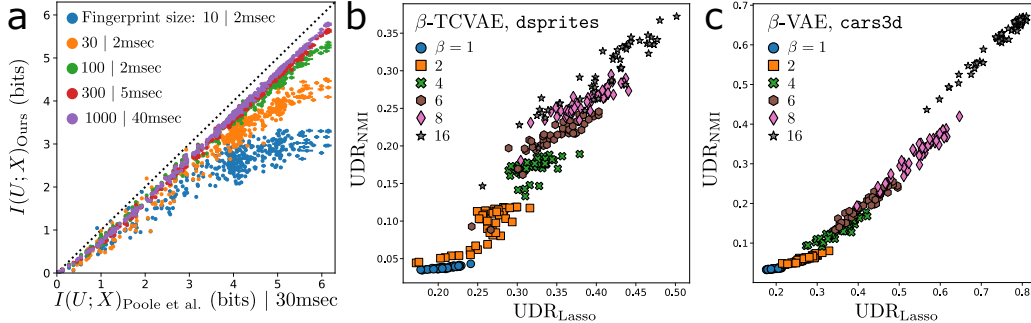


Figure 3: **Benchmarking mutual information estimation and model similarity.** (a) On 500 latent dimensions randomly sampled from a variety of VAE models trained on the `dsprites` dataset, the transmitted information $I(X; U)$ was estimated with both the BC matrices and the bounds from Poole et al. [50]. Each point is a different channel from the set of learned models, and the colors indicate the size of the data sample used for the BC matrices. Horizontal error bars span the lower to the upper bound estimates. (b,c) We replace the measure of channel similarity in UDR [11] to NMI, for two sets of models trained by Locatello et al. [1].

that are based on modelling, such as UDR [11] or ModelCentrality [8], the statistical similarity used in this work requires only differentiable operations and can thus be optimized. We optimize a synthesis channel by minimizing its distance to a set of reference channels, performing gradient descent directly on the encoding of the data points used for the Bhattacharyya matrices. Instead of requiring several models to be in memory during training of a new encoder, the Bhattacharyya matrices are computed for the ensemble channels once and then used for comparison during training, all with efficient array operations to make training practical.

4 Experiments

4.1 Improving the measure of similarity in unsupervised disentanglement ranking (UDR)

We first performed a sanity check for the treatment of representation (sub)spaces as soft clustering and for the proposed extensions of NMI and VI to soft clustering schemes. We replaced the measure of similarity between channels in UDR [11] with NMI or $\exp(-VI)$ and left the rest of the computation of UDR intact. In contrast to the original measures of similarity, NMI and VI properly account for the nature of embeddings as distributions, allow information content to be directly assessed, and are not restricted to one-dimensional spaces. The behavior of UDR is largely preserved, though with enhanced discerning power between model hyperparameters with NMI (Fig. 3b,c; additional results using NMI and VI in Appx. D). The results support our methodology to compare representation spaces, though we note an important high-level shift in focus from previous model-centric measures of disentanglement to the current work’s channel-centric view. By revealing the pieces of information repeatedly found in an ensemble, we illuminate the process of information fragmentation and the effect of inductive biases, something missed by an assessment based on model-to-model comparisons.

4.2 Unsupervised detection of structure: synthetic datasets

We analyzed the information content of ensembles of VAEs on classic disentanglement datasets where generative factors are available for evaluation, and where the data consists of every possible combination of the factors without correlations. Using fifty models with ten channels (dimensions) each, for a variety of datasets, models, and hyperparameters released with Locatello et al. [1]¹, we assessed structure in sets of 500 channels using the generalized similarity measures and density-based clustering. Before applying OPTICS, we removed channels transmitting less than 0.01 bits of information. We found NMI to be better at detecting structure than VI and focus on it in the following (discussion in Appx. B).

In Fig. 4, we show a representative sampling of analyses that can be performed with the proposed method; additional results are in Appx. A. The matrices display the pairwise NMI between all

¹https://github.com/google-research/disentanglement_lib/tree/master

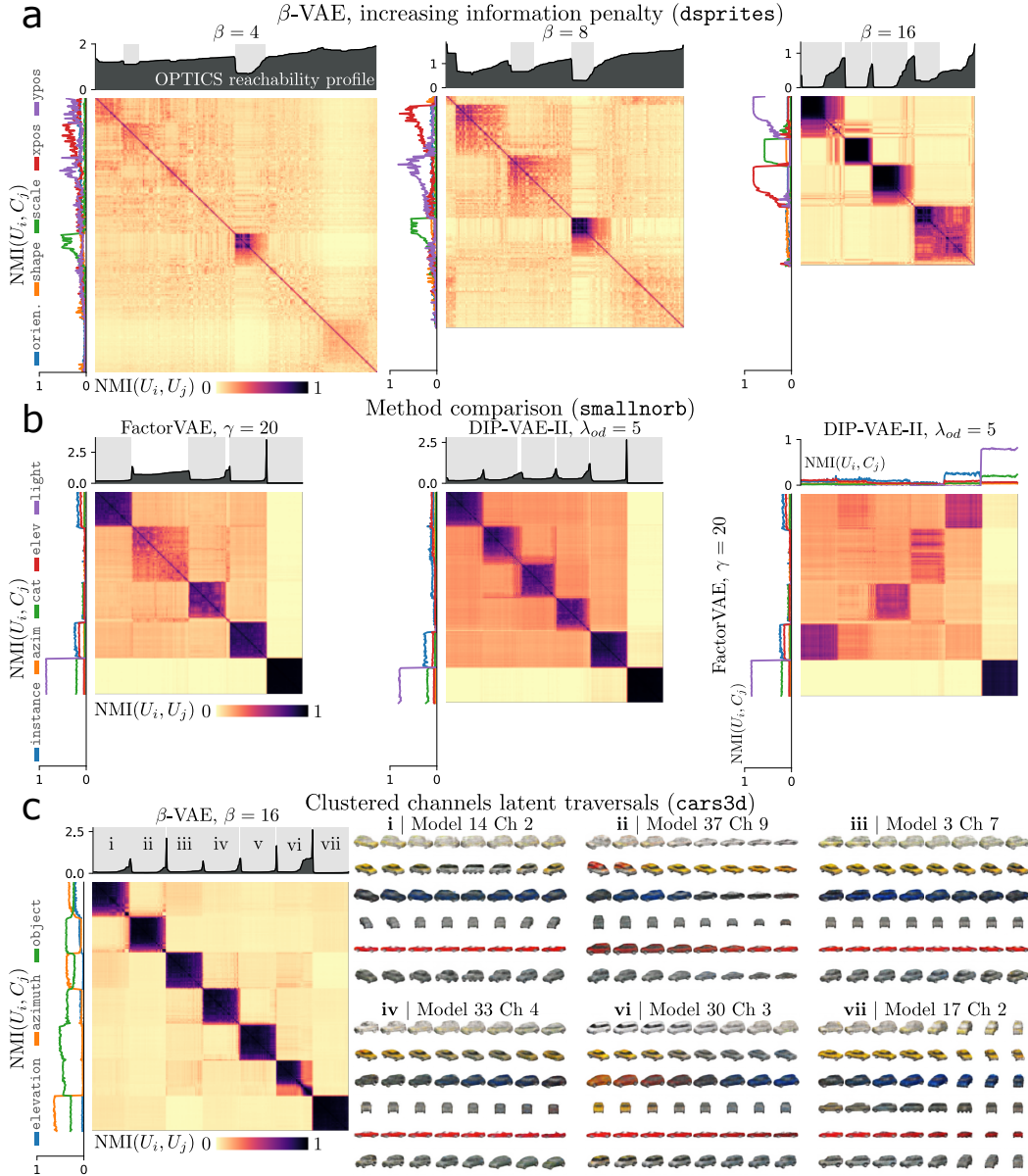


Figure 4: **Structure in the learned channels from 50 models.** We visualize the structure found in ensembles as (a) the information penalty of a β -VAE is increased on dsprites, and (b) the method is varied with similar amounts of informative channels on smallnorb. (c) Latent traversals for the most central channel to each grouping, labelled with lowercase Roman numerals, found for β -VAE trained on cars3d. Grouping v can be found in Appx. A. All matrices are sized to 383×383 , the number of informative channels of the $\beta = 4$ β -VAE on dsprites.

informative channels in the ensemble, and have been reorganized by the OPTICS algorithm such that dense regions of channels appear as block diagonal matrices. On the left of each channel similarity matrix is the NMI with the ground truth generative factors, and above is the reachability profile where dense regions are indicated by valleys and identified groupings of channels by shading.

In Fig. 4a, the regularization of a β -VAE is increased for the dsprites dataset [53]. Although there are more channels that convey information for lower regularization ($\beta=4$), there is little discernible structure in the population of channels aside from a group of channels that roughly communicate the

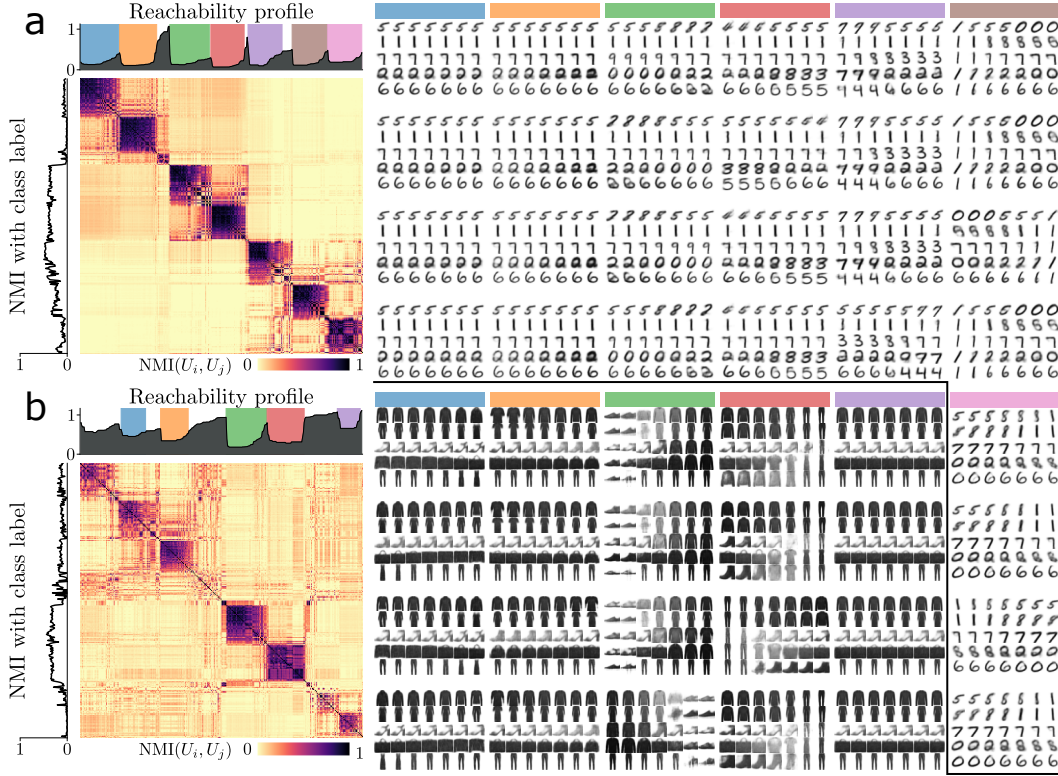


Figure 5: **Channel structure on MNIST, Fashion-MNIST.** Channel similarity analysis for 50 β -VAEs trained on MNIST (a), $\beta=8$, and Fashion-MNIST (b), $\beta = 4$. The most central four channels to each of the found groupings (indicated by colors) are visualized via latent traversal on the right.

same scale information. As β increases, a block diagonal structure is found, and channels with the same x_{pos} , y_{pos} , and scale information are found repeatedly across runs in the ensemble.

Fig. 4b compares the channel similarity structure found by different methods of regularization on the `smallnorb` dataset [54]. While a block diagonal structure is found for both, indicating consistent information fragmentation, are the information fragments the same for the two methods? After reorganizing the channels for each method with OPTICS, we can compare the channels to each other, computing the NMI between all channels found by FactorVAE [8] and those by DIP-VAE [55]. The fragment with lighting information is consistent across methods, but the other fragments are less so, and we identify a fragment found by DIP-VAE that is not found by FactorVAE.

Finally, Fig. 4c visualizes the information content of found groupings of channels via latent traversals. Given a group of channels identified by OPTICS, we take as a representative the channel that maximizes the average similarity to others in the group. Information fragmentation on the `cars3d` dataset [56] is highly consistent, though not in the manner that the generative factors are siloed. For instance, the object factor is broken repeatedly into the same set of fragments. Additionally surprising is that some fragments of the object factor are consistently mixed with information about the pose. In cluster i, a specific combination of information from all three factors is repeatedly found, and the corresponding latent traversals shows some color information mixed with azimuth and elevation. Cluster iv also combines azimuth and color information, indicating a particular way of fragmenting information combining these factors that is consistent across repeat training runs. The remaining commonly found channels are more straightforward to interpret.

4.3 Unsupervised detection of structure: in the wild

We now leave the realm of synthetic datasets and analyze structure in ensembles of β -VAEs trained on MNIST [57] ($\beta=8$) and fashion-MNIST [58] ($\beta=4$) (Fig. 5). Besides class labels, the remaining variation in these datasets, which we refer to as style, is not well-defined. Nevertheless, we found that

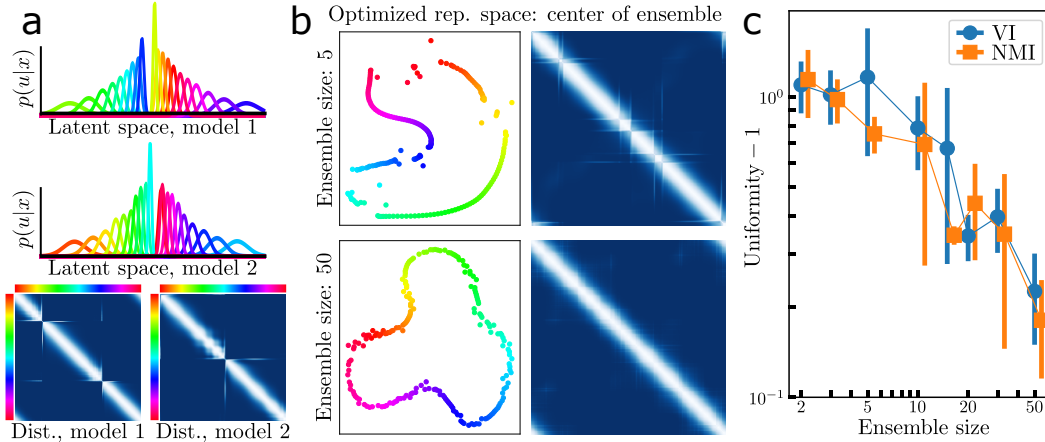


Figure 6: **Ensemble learning of a factor with $SO(2)$ structure via 50 weak learners.** A dataset is generated from a single periodic factor that we represent as color hue. (a) A β -VAE with a one-dimensional latent space cannot represent the periodic structure of the generative factor, and must contain ‘scars’, shown in the posteriors (top) and the distinguishability matrix (bottom) for two example latent spaces. (b) We directly optimize latent encodings for 200 points in a two-dimensional space, and maximize the channel’s similarity (either NMI or $\exp(-VI)$) with the ensemble of five (top) and fifty (bottom) models. We display the centers of the posterior distributions on the left. (c) The uniformity of neighbor distances, a proxy for the periodic global structure of the generative factor, averaged over five repeats of the experiment. Error bars are standard deviation over the repeats.

variation is fragmented in a fairly consistent manner for both datasets. In MNIST (Fig. 5a), seven clusters were found that split class and style information into largely similar pieces. We display latent traversals for several channels that were centrally located in each cluster, and find that nearly identical traversals are found again and again. Channels in the blue cluster seem to convey information only about the tail of 2s, while those in the orange cluster convey class-invariant information about stroke thickness. The remaining clusters convey more class information. Channels trained on Fashion-MNIST (Fig. 5) similarly fragment information into remarkably consistent—though not necessarily intuitive—pieces. The green group, for example, communicates information to distinguish between shoes and others, while the red group of channels distinguishes pants from others.

4.4 Ensemble learning in a toy example

Finally, we created a toy example to demonstrate the ability to do ensemble learning with the proposed method. Consider a dataset with a single generative factor with $SO(2)$ symmetry, such as an object’s hue (Fig. 6). We trained an ensemble of β -VAEs, each with a one-dimensional latent space that was insufficient to represent the global structure of the generative factor. In Fig. 6a, we show two example latent spaces and their associated distinguishability matrices. The matrices highlight the ‘scars’ in the latent space where similar values of the generative factor are dissimilar in latent space. While a latent space with one scar is possible, most models became stuck in local minima with two scars.

We used the ensemble of Bhattacharyya distinguishability matrices from the ensemble to perform gradient descent directly on point embeddings in a 2D latent space whose distinguishability matrix maximized similarity with the ensemble. Namely, we used either NMI or the $\exp(-VI)$, between the optimizable Bhattacharyya matrix—recomputed every batch—and those of the ensemble. As more 1D latent spaces are added to the ensemble, the optimized 2D latent space smooths out and captures the global structure of the generative factor (Fig. 6b). We quantify the performance improvement by measuring the uniformity of spacing between embedded means of adjacent values in the generative factor. Specifically, we use the standard deviation of the Euclidean distances between the posterior means of these neighboring points divided by the mean neighbor distance (Fig. 6c). Both NMI and VI boost an ensemble of weak learners to represent the generative factor, with improved accuracy for larger ensembles.

5 Discussion

The proposed methodology relies on training ensembles of models for each hyperparameter setting, making computational costs an important consideration. We found 50 models per ensemble to be sufficient to assess structure, and further found that there is much to learn from ensembles of relatively weak models. On our machine with public code, training a single model from a recently proposed method (QLAE, Hsu et al. [10]) took more than five hours, whereas we could train more than ten β -VAEs with simpler architectures in the same time. As demonstrated in Sec. 4.4 with the toy problem, ensemble learning with weak models that are fast to train offers a promising alternative to disentanglement with larger and more complicated models.

The proposed analysis is computationally lightweight. Distinguishability matrices can be saved during training and used for all downstream analysis. Importantly, by representing the information content of a channel with distinguishability matrices, the downstream analysis of structure is agnostic to the dimensionality of the channels, their discrete or continuous nature, and even whether the channels were side information attached to the dataset in the form of labels.

New directions of disentanglement research open when shifting the focus of evaluation from “how well did the model achieve some specific form of disentanglement?” to a more empirical “how did this model split information about the data?” How do different inductive biases influence the way information is fragmented into channels? Why is information about car model in the `cars3d` dataset or digit class in MNIST consistently split into the same pieces? By understanding the way different inductive biases and other methodological considerations influence the way information is fragmented into channels, we gain a deeper understanding of the nature of disentanglement and thus more capacity to engineer it.

Limitations. Assessing structure in high-dimensional data is difficult, in part due to the sensitivity to every aspect of the analysis—from the measure of similarity/distance to the algorithm used. We have made reasonable extensions to two classic measures of similarity between clusterings, and used one particular density-based clustering algorithm—OPTICS [51]—to discover repeatedly found fragments of information. Care must be taken to not over-interpret the results, as in any scenario where structure in high-dimensional data is assessed via dimensionality reduction.

References

- [1] Francesco Locatello, Stefan Bauer, Mario Lucic, Gunnar Raetsch, Sylvain Gelly, Bernhard Schölkopf, and Olivier Bachem. Challenging common assumptions in the unsupervised learning of disentangled representations. In *international conference on machine learning*, pages 4114–4124. PMLR, 2019. 1, 2, 3, 5, 6, 14, 20, 21
- [2] Christoph Molnar. *Interpretable Machine Learning: A Guide for Making Black Box Models Explainable*. 2022. 1
- [3] Frederik Träuble, Elliot Creager, Niki Kilbertus, Francesco Locatello, Andrea Dittadi, Anirudh Goyal, Bernhard Schölkopf, and Stefan Bauer. On disentangled representations learned from correlated data. In *International Conference on Machine Learning*, pages 10401–10412. PMLR, 2021. 1
- [4] Irina Higgins, David Amos, David Pfau, Sebastien Racaniere, Loic Matthey, Danilo Rezende, and Alexander Lerchner. Towards a definition of disentangled representations. *arXiv preprint arXiv:1812.02230*, 2018. 1
- [5] Nikita Balabin, Daria Voronkova, Ilya Trofimov, Evgeny Burnaev, and Serguei Barannikov. Disentanglement learning via topology. *arXiv preprint arXiv:2308.12696*, 2023. 1, 3
- [6] Sjoerd Van Steenkiste, Francesco Locatello, Jürgen Schmidhuber, and Olivier Bachem. Are disentangled representations helpful for abstract visual reasoning? *Advances in neural information processing systems*, 32, 2019. 1
- [7] Ricky TQ Chen, Xuechen Li, Roger B Grosse, and David K Duvenaud. Isolating sources of disentanglement in variational autoencoders. *Advances in neural information processing systems*, 31, 2018. 1, 3

- [8] Hyunjik Kim and Andriy Mnih. Disentangling by factorising. In *International conference on machine learning*, pages 2649–2658. PMLR, 2018. 3, 6, 8
- [9] Cian Eastwood and Christopher KI Williams. A framework for the quantitative evaluation of disentangled representations. In *International conference on learning representations*, 2018. 3
- [10] Kyle Hsu, Will Dorrell, James C. R. Whittington, Jiajun Wu, and Chelsea Finn. Disentanglement via latent quantization. In *Neural Information Processing Systems*, 2023. 1, 3, 10
- [11] Sunny Duan, Loic Matthey, Andre Saraiva, Nick Watters, Chris Burgess, Alexander Lerchner, and Irina Higgins. Unsupervised model selection for variational disentangled representation learning. In *International Conference on Learning Representations*, 2020. 1, 2, 3, 6, 19, 20, 21
- [12] Zinan Lin, Kiran Thekumparampil, Giulia Fanti, and Sewoong Oh. Infogan-cr and modelcentrality: Self-supervised model training and selection for disentangling gans. In *international conference on machine learning*, pages 6127–6139. PMLR, 2020. 1, 3
- [13] Kunal Punera and Joydeep Ghosh. Soft cluster ensembles. *Advances in fuzzy clustering and its applications*, pages 69–90, 2007. 2, 3
- [14] Alexander Strehl and Joydeep Ghosh. Cluster ensembles—a knowledge reuse framework for combining multiple partitions. *Journal of machine learning research*, 3(Dec):583–617, 2002. 2, 4, 5
- [15] Silke Wagner and Dorothea Wagner. Comparing clusterings: an overview. 2007. 2
- [16] Nguyen Xuan Vinh, Julien Epps, and James Bailey. Information theoretic measures for clusterings comparison: is a correction for chance necessary? In *Proceedings of the 26th annual international conference on machine learning*, pages 1073–1080, 2009.
- [17] Nguyen Xuan Vinh, Julien Epps, and James Bailey. Information theoretic measures for clusterings comparison: Variants, properties, normalization and correction for chance. *Journal of Machine Learning Research*, 11(95):2837–2854, 2010. URL <http://jmlr.org/papers/v11/vinh10a.html>.
- [18] Sandro Vega-Pons and José Ruiz-Shulcloper. A survey of clustering ensemble algorithms. *International Journal of Pattern Recognition and Artificial Intelligence*, 25(03):337–372, 2011.
- [19] Dong Huang, Chang-Dong Wang, and Jian-Huang Lai. Locally weighted ensemble clustering. *IEEE transactions on cybernetics*, 48(5):1460–1473, 2017. 2
- [20] Marina Meilă. Comparing clusterings by the variation of information. In *Learning Theory and Kernel Machines: 16th Annual Conference on Learning Theory and 7th Kernel Workshop, COLT/Kernel 2003, Washington, DC, USA, August 24-27, 2003. Proceedings*, pages 173–187. Springer, 2003. 2, 4
- [21] Claude Shannon. The lattice theory of information. *Transactions of the IRE professional Group on Information Theory*, 1(1):105–107, 1953. 2
- [22] James P Crutchfield. Information and its metric. In *Nonlinear Structures in Physical Systems: Pattern Formation, Chaos, and Waves Proceedings of the Second Woodward Conference San Jose State University November 17–18, 1989*, pages 119–130. Springer, 1990. 2
- [23] Andrea Campagner, Davide Ciucci, and Thierry Dencœux. A general framework for evaluating and comparing soft clusterings. *Information Sciences*, 623:70–93, 2023. 2, 3
- [24] Lotfi Asker Zadeh. Fuzzy sets. *Information and control*, 8(3):338–353, 1965. 3, 4
- [25] Joseph C Dunn. A fuzzy relative of the isodata process and its use in detecting compact well-separated clusters. 1973.
- [26] Enrique H Ruspini, James C Bezdek, and James M Keller. Fuzzy clustering: A historical perspective. *IEEE Computational Intelligence Magazine*, 14(1):45–55, 2019. 3, 4

- [27] Eyke Hullermeier, Maria Rifqi, Sascha Henzgen, and Robin Senge. Comparing fuzzy partitions: A generalization of the rand index and related measures. *IEEE Transactions on Fuzzy Systems*, 20(3):546–556, 2011. 3
- [28] Antonio D’Ambrosio, Sonia Amodio, Carmela Iorio, Giuseppe Pandolfo, and Roberta Siciliano. Adjusted concordance index: an extension of the adjusted rand index to fuzzy partitions. *Journal of Classification*, 38:112–128, 2021.
- [29] Jeffrey L Andrews, Ryan Browne, and Chelsey D Hvingelby. On assessments of agreement between fuzzy partitions. *Journal of Classification*, 39(2):326–342, 2022.
- [30] Hong-Yu Wang, Jie-Sheng Wang, and Guan Wang. A survey of fuzzy clustering validity evaluation methods. *Information Sciences*, 618:270–297, 2022. 3
- [31] Andrea Campagner and Davide Ciucci. Orthopartitions and soft clustering: soft mutual information measures for clustering validation. *Knowledge-Based Systems*, 180:51–61, 2019. 3
- [32] Simon Kornblith, Mohammad Norouzi, Honglak Lee, and Geoffrey Hinton. Similarity of neural network representations revisited. In *International conference on machine learning*, pages 3519–3529. PMLR, 2019. 3
- [33] Katherine Hermann and Andrew Lampinen. What shapes feature representations? exploring datasets, architectures, and training. *Advances in Neural Information Processing Systems*, 33: 9995–10006, 2020.
- [34] Alex H Williams, Erin Kunz, Simon Kornblith, and Scott Linderman. Generalized shape metrics on neural representations. *Advances in Neural Information Processing Systems*, 34:4738–4750, 2021. 3
- [35] Nikolaus Kriegeskorte, Marieke Mur, and Peter A Bandettini. Representational similarity analysis-connecting the branches of systems neuroscience. *Frontiers in systems neuroscience*, 2:249, 2008. 3
- [36] Ilyes Khemakhem, Diederik Kingma, Ricardo Monti, and Aapo Hyvarinen. Variational autoencoders and nonlinear ica: A unifying framework. In *International Conference on Artificial Intelligence and Statistics*, pages 2207–2217. PMLR, 2020. 3
- [37] Eduardo Hugo Sanchez, Mathieu Serrurier, and Mathias Ortner. Learning disentangled representations via mutual information estimation. In *The European Conference on Computer Vision (ECCV)*, 2020.
- [38] Matthew J Vowels, Necati Cihan Camgoz, and Richard Bowden. Nestedvae: Isolating common factors via weak supervision. In *Proceedings of the IEEE/CVF Conference on Computer Vision and Pattern Recognition*, pages 9202–9212, 2020.
- [39] Kieran A Murphy, Varun Jampani, Srikumar Ramalingam, and Ameesh Makadia. Learning abcs: Approximate bijective correspondence for isolating factors of variation with weak supervision. In *Proceedings of the IEEE/CVF Conference on Computer Vision and Pattern Recognition*, pages 16010–16020, 2022. 3
- [40] Michal Rolínek, Dominik Zietlow, and Georg Martius. Variational autoencoders pursue pca directions (by accident). In *Proceedings of the IEEE/CVF Conference on Computer Vision and Pattern Recognition*, pages 12406–12415, 2019. 3, 14
- [41] Dominik Zietlow, Michal Rolínek, and Georg Martius. Demystifying inductive biases for (beta-)vae based architectures. In Marina Meila and Tong Zhang, editors, *Proceedings of the 38th International Conference on Machine Learning*, volume 139 of *Proceedings of Machine Learning Research*, pages 12945–12954. PMLR, 18–24 Jul 2021. URL <https://proceedings.mlr.press/v139/zietlow21a.html>.
- [42] Kyle Hsu, Jubayer Ibn Hamid, Kaylee Burns, Chelsea Finn, and Jiajun Wu. Tripod: Three complementary inductive biases for disentangled representation learning. *arXiv preprint arXiv:2404.10282*, 2024. 3

- [43] Benjamin Estermann and Roger Wattenhofer. Dava: Disentangling adversarial variational autoencoder. In *International Conference on Learning Representations (ICLR)*, 2023. 3
- [44] Diederik P. Kingma and Max Welling. Auto-encoding variational Bayes. In *International Conference on Learning Representations (ICLR)*, 2014. 3
- [45] Thomas M Cover and Joy A Thomas. *Elements of information theory*. John Wiley & Sons, 1999. 3
- [46] Alexander A. Alemi, Ian Fischer, Joshua V. Dillon, and Kevin Murphy. Deep variational information bottleneck. *International Conference on Learning Representations (ICLR)*, 2017. 3
- [47] Thomas Kailath. The divergence and bhattacharyya distance measures in signal selection. *IEEE transactions on communication technology*, 15(1):52–60, 1967. 4
- [48] Kieran A Murphy and Dani S. Bassett. Interpretability with full complexity by constraining feature information. In *International Conference on Learning Representations (ICLR)*, 2023. URL https://openreview.net/forum?id=R_OL5mLhsv. 4
- [49] Artemy Kolchinsky and Brendan D Tracey. Estimating mixture entropy with pairwise distances. *Entropy*, 19(7):361, 2017. 5, 18
- [50] Ben Poole, Sherjil Ozair, Aaron Van Den Oord, Alex Alemi, and George Tucker. On variational bounds of mutual information. In *International Conference on Machine Learning*, pages 5171–5180. PMLR, 2019. URL <https://proceedings.mlr.press/v97/poole19a/poole19a.pdf>. 5, 6
- [51] Mihael Ankerst, Markus M Breunig, Hans-Peter Kriegel, and Jörg Sander. Optics: Ordering points to identify the clustering structure. *ACM Sigmod record*, 28(2):49–60, 1999. 5, 10
- [52] Jörg Sander, Xuejie Qin, Zhiyong Lu, Nan Niu, and Alex Kovarsky. Automatic extraction of clusters from hierarchical clustering representations. In *Advances in Knowledge Discovery and Data Mining: 7th Pacific-Asia Conference, PAKDD 2003, Seoul, Korea, April 30–May 2, 2003 Proceedings 7*, pages 75–87. Springer, 2003. 5
- [53] Irina Higgins, Loïc Matthey, Arka Pal, Christopher Burgess, Xavier Glorot, Matthew Botvinick, Shakir Mohamed, and Alexander Lerchner. beta-vae: Learning basic visual concepts with a constrained variational framework. In *International Conference on Learning Representations (ICLR)*, 2017. 7
- [54] Yann LeCun, Fu Jie Huang, and Leon Bottou. Learning methods for generic object recognition with invariance to pose and lighting. In *Proceedings of the 2004 IEEE Computer Society Conference on Computer Vision and Pattern Recognition, 2004. CVPR 2004.*, volume 2, pages II–104. IEEE, 2004. 8
- [55] Abhishek Kumar, Prasanna Sattigeri, and Avinash Balakrishnan. Variational inference of disentangled latent concepts from unlabeled observations. In *International Conference on Learning Representations*, 2018. URL <https://openreview.net/forum?id=H1kG7GZAW>. 8
- [56] Scott E Reed, Yi Zhang, Yuting Zhang, and Honglak Lee. Deep visual analogy-making. *Advances in neural information processing systems*, 28, 2015. 8
- [57] Yann LeCun, Corinna Cortes, and CJ Burges. Mnist handwritten digit database. *ATT Labs [Online]*. Available: <http://yann.lecun.com/exdb/mnist>, 2, 2010. 8
- [58] Han Xiao, Kashif Rasul, and Roland Vollgraf. Fashion-mnist: a novel image dataset for benchmarking machine learning algorithms. *arXiv preprint arXiv:1708.07747*, 2017. 8
- [59] Christopher P Burgess, Irina Higgins, Arka Pal, Loic Matthey, Nick Watters, Guillaume Desjardins, and Alexander Lerchner. Understanding disentangling in β -VAE. *arXiv preprint arXiv:1804.03599*, 2018. 19

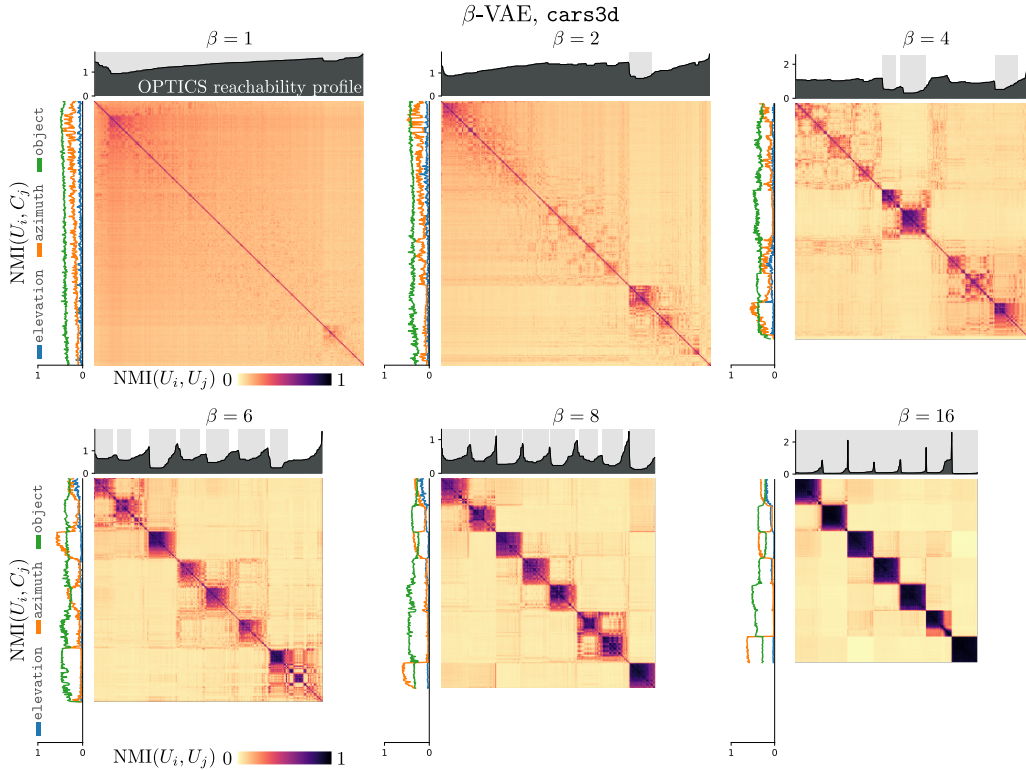


Figure 7: Extended structure visualizations for cars3d, β -VAE.

A Appendix: Extended clustering results

In Figs. 7, 8, and 9, we repeat the structural analysis of Sec. 4.2 with all β -VAE hyperparameters explored by the authors of Locatello et al. [1]. The effect of increasing β is clearly observed by the emergence of block diagonal channel similarity matrices, though with fewer informative channels with increased β .

Consider the cars3d ensembles in Fig. 7. With $\beta = 1, 2$, the information fragmentation is not consistent across repeat runs, even though the amount of information shared with the three generative factors is fairly consistent. This highlights the value of directly comparing the information content of channels with NMI or VI—instead of comparing indirectly via information content about known generative factors—with the added benefit of being fully unsupervised, requiring no ground truth factors. For $\beta = 4$ the learned fragments of information start to coalesce, with information regularization breaking the degeneracy that plagues unsupervised disentanglement [1]. For $\beta = 8, 16$, the regularization is strong enough to form consistent fragments of information across random initializations. What about the specific form of information regularization and the implicit inductive biases [40] caused the three factors to be robustly fragmented in this specific manner and not another?

In Fig. 10 we replicate Fig. 4 with VI as the input to the OPTICS algorithm instead of $-\log(\text{NMI})$. Much of the block diagonal structure is found with either method of assessing distance between channels, though additional structure was found with NMI for dsprites $\beta = 4, 8$ that was not detected with VI.

Finally, in Fig. 11 we present additional latent traversals for the cars3d channel groupings presented in Fig. 4c. With the channels most centrally located in each group (as before), we also display latent traversals for a randomly selected channel in each group in order to convey the uniformity of the information content within each group. As before, the models used for this analysis are publicly available, released with Locatello et al. [1], allowing the traversals here to be reproduced by downloading the model whose index is the model number plus 9250 (the index offset for cars3d, β -VAE with $\beta = 16$) and traversing the appropriate channel (zero-indexed).

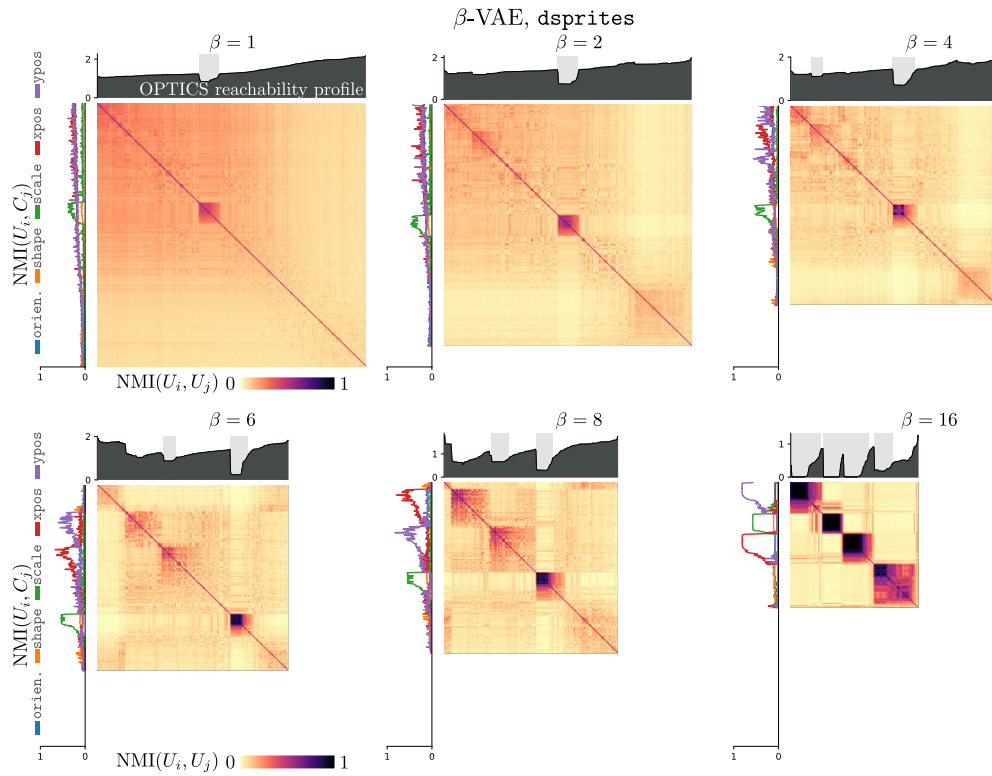


Figure 8: Extended structure visualizations for dsprites, β -VAE.

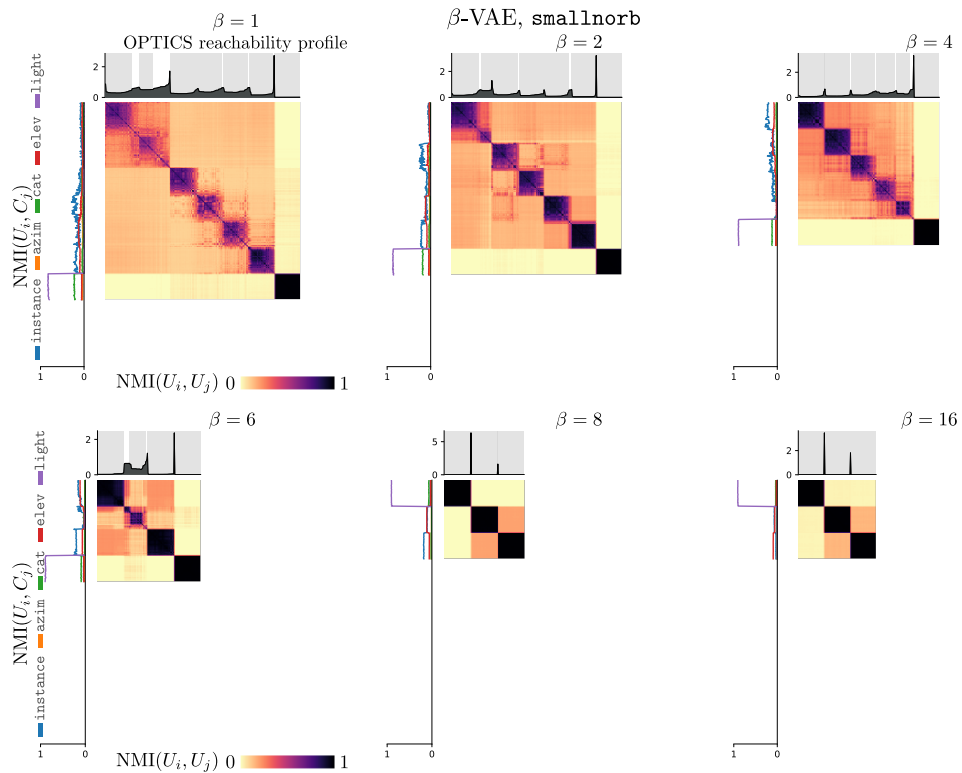


Figure 9: Extended structure visualizations for smallnorb, β -VAE.

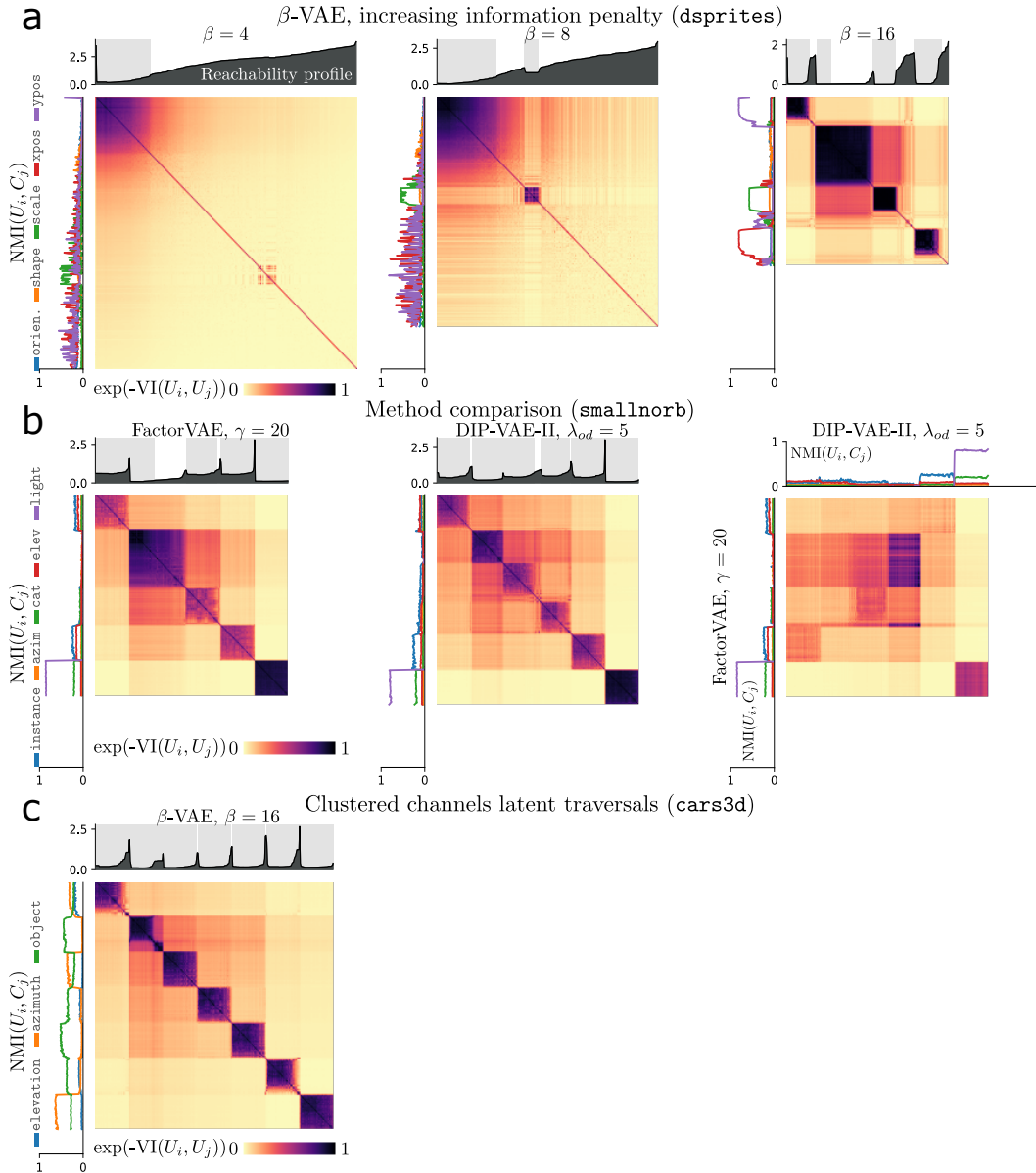


Figure 10: **Structure in the learned channels from 50 models, using VI.** Analogue of Fig. 4 in the main text, where clustering is by VI and we display the pairwise similarity according to VI (the exponentiated negative VI) instead of NMI. We visualize the structure found in ensembles as (a) the information penalty of a β -VAE is increased on dsprites, and (b) the method is varied with approximately the same information transmission on smallnorb, (c) and robust groupings are found with a β -VAE on cars3d.

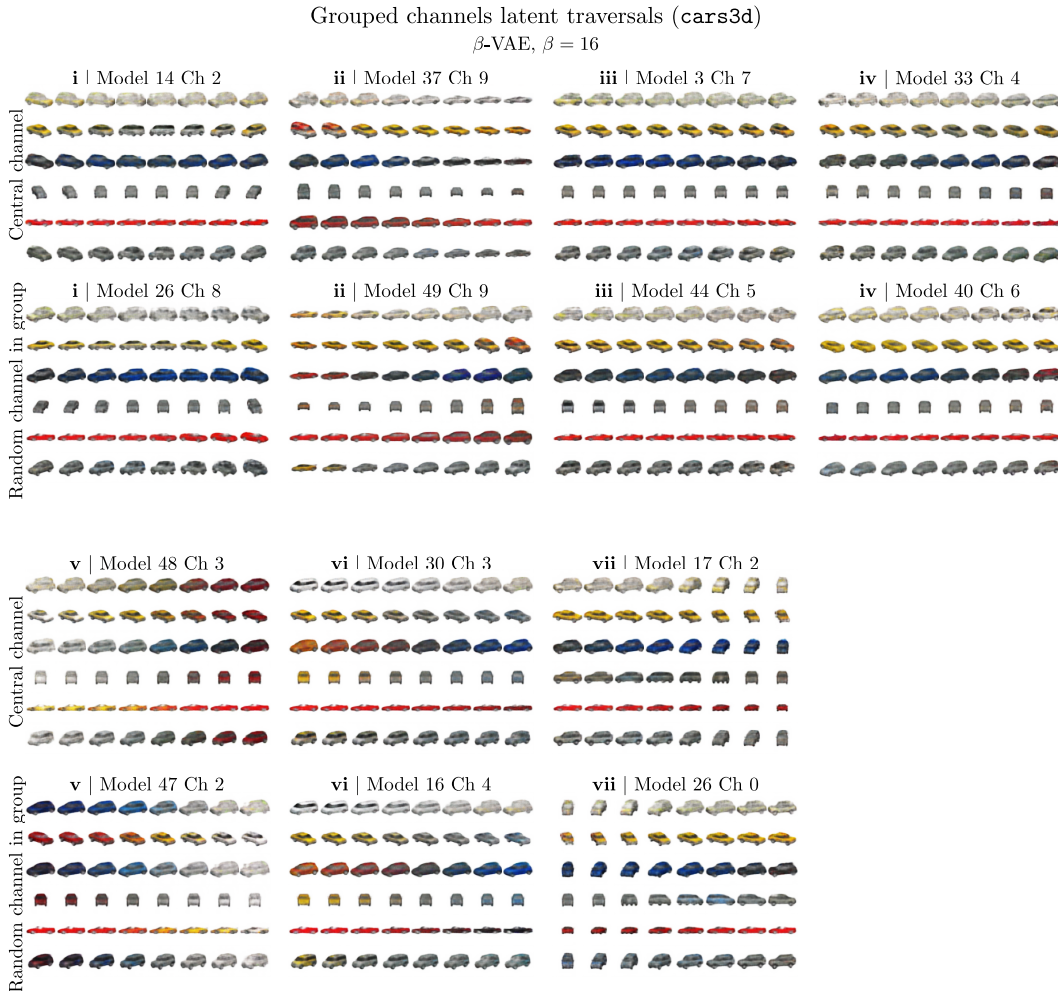


Figure 11: **Extended latent traversals for *cars3d* groups from Fig. 4c.** For all seven groupings of channels found in Fig. 4c, we display latent traversals for the most central channel and a randomly selected channel from the grouping. Traversals are over the range $[-2, 2]$.

B Appendix: Are NMI and VI interchangeable?

NMI and VI, aside from the inversion required to convert from similarity to distance, involve many of the same mutual information terms and bear some resemblance when ignoring the normalization factor for NMI. Are they interchangeable, or do they assess structure differently?

In Fig. 12, we compare NMI and VI directly as similarity or distance measures for the pairwise comparisons between channels used in Fig. 4. Specifically, as measures of similarity, we plot NMI against $\exp(-VI)$, and for distance we plot $-\log(NMI)$ against VI. We find that NMI and VI are non-trivially related, shown clearly by the horizontal and vertical swaths of points where one of the two measures is roughly constant while the other varies considerably. Consider the top row, with the ensembles for $\beta = 4, 8$ dsprites β -VAEs: NMI is low for the majority of channel pairs while

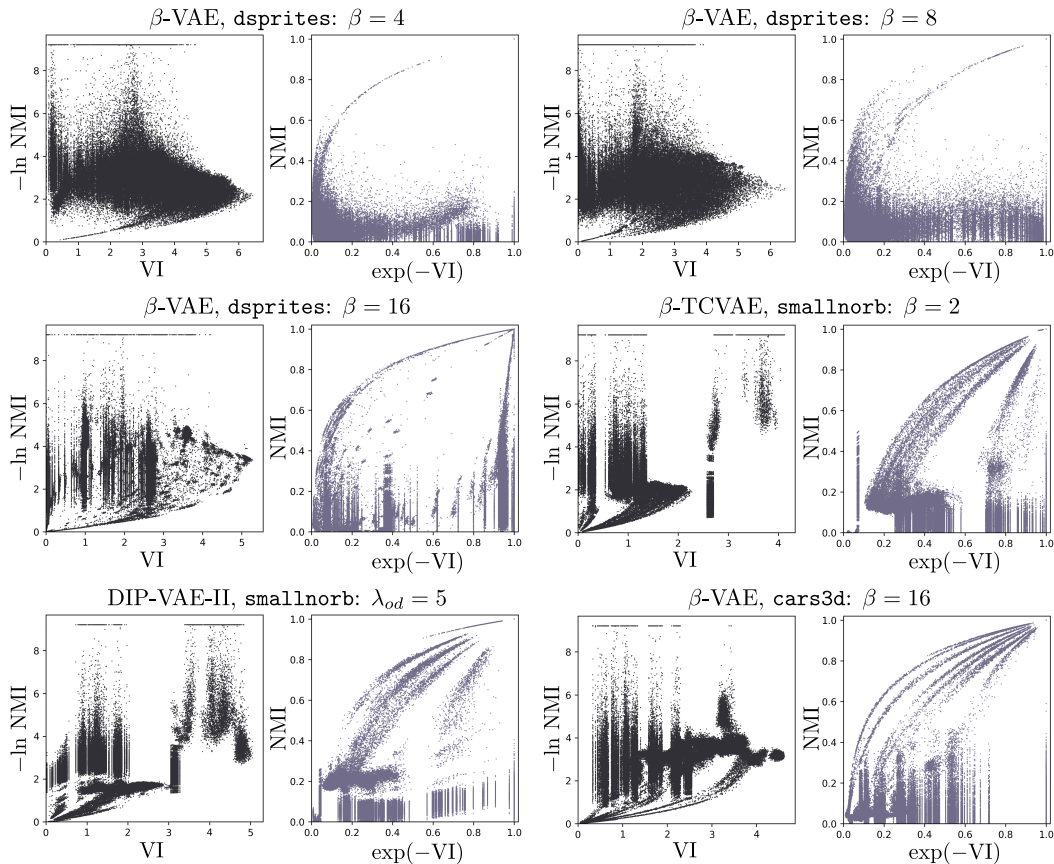


Figure 12: **Direct comparison of NMI and VI.** We convert both measures to a distance measure (black) and to a similarity measure (blue gray) and compare them for the pairwise channel comparisons from the ensembles of Fig. 4.

VI spans its range. By assigning high similarity (resp., low distance) to fewer pairs of channels, NMI detected more structure in the $\beta = 4, 8$ dsprites β -VAE ensembles (Fig. 4a,b) than did VI (Fig. 10a,b), which is why we opted to use it in the main text. After the hot spots solidified, both VI and NMI identified structure similarly (the rest of Fig. 4 and Fig. 10). Interestingly, the corresponding NMI and VI comparisons in Fig. 12 show multiple distinct arcs of channel similarity, as well as clear vertical bands where NMI has discerning power and VI does not.

C Appendix: Assumptions for information estimation using Bhattacharyya distinguishability matrices

To estimate the mutual information $I(U; X)$ from the Bhattacharyya distinguishability matrices, we have employed the lower bound derived in Kolchinsky and Tracey [49] for the information communicated through a channel about a mixture distribution (following the most updated version on arXiv²). The bound simplifies greatly when the empirical distribution is assumed to be a reasonable approximation for the data distribution, and then we further assume the sample of data used for the fingerprint allows for an adequate approximation of the marginal distribution in latent space. First we reproduce the bound from Sec. V of Kolchinsky and Tracey [49] using the notation of this work, and then we describe our assumptions to apply the bound as an estimate of the information contained in a probabilistic representation space.

²<https://arxiv.org/abs/1706.02419>

Let X be the input to a channel, following a mixture distribution with N components, $x \sim p(x) = \sum_{i=1}^N c_i p_i(x)$, and U the output of the same channel, $u \sim p(u) = \sum_{i=1}^N c_i (\int_{\mathcal{X}} p(u|x) p_i(x) dx)$. Then we have

$$I(X; U) \geq - \sum_i c_i \ln \sum_j c_j BC_{ij} + H(U|C) - H(U|X), \quad (5)$$

where C is a random variable representing the component identity.

In this work, we assume that the data distribution can be approximated by the empirical distribution, $p(x) \approx \sum_i^N \delta(x - x_i)/N$, simplifying Eqn. 5 so that $c_i \equiv 1/N$ and $H(U|C) = H(U|X)$ because the identity of the component is equivalent to the identity of the datum. Finally, we assume that the set of posterior distributions for a representative sample of size M of the dataset, taken for the fingerprint, adequately approximates the empirical distribution. Larger samples may be necessary in different scenarios, for example when the amount of information transmitted by channels is larger than a handful of bits, but $M = 1000$ appeared sufficient for the analyses of this work.

The corrections to NMI and VI required the information conveyed by two measurements from different channels, $I(X; U, V)$ as well as from the same channel, $I(X; U, U')$. The matrix of Bhattacharyya coefficients given measurements U and V is simply the elementwise product of the coefficients given U and the coefficients given V . The posterior in the joint space of U and V is factorizable given x —i.e., $p(u, v|x) = p(u|x)p(v|x)$ —because the stochasticity in each channel is independent. The same is true for the joint space of U and U' , two draws from the same channel. The Bhattacharyya coefficient of the joint variable simplifies,

$$\begin{aligned} BC_{ij}^{UV} &= \int_{\mathcal{U}} \int_{\mathcal{V}} \sqrt{p(u, v|x_i)p(u, v|x_j)} dudv \\ &= \int_{\mathcal{U}} \sqrt{p(u|x_i)p(u|x_j)} du \int_{\mathcal{V}} \sqrt{p(v|x_i)p(v|x_j)} dv \\ &= BC_{ij}^U \times BC_{ij}^V. \end{aligned} \quad (6)$$

D Appendix: Extended UDR comparisons

Here we include additional comparisons between UDR [11] (Figs. 13 and 14) where the channel-wise similarity is calculated with either the coefficients of a Lasso model as originally proposed, or with NMI or $\exp(-VI)$. As stated in the main text, there is general agreement between the proposed measures of channel similarity and the original UDR. For β -TCVAE, both NMI and VI grant UDR more discerning power between different hyperparameters—and even within runs of the same hyperparameter, see $\beta = 2$ for `dsprites`—than Lasso. This can be seen as vertical ranges with little or no overlap between hyperparameters, while horizontal ranges contain significant overlap such that a single value of UDR_{Lasso} would not tell which of two hyperparameters was run.

Another point of disagreement is for the Annealed VAE (or CCI-VAE) [59]. The information content of the learned latent spaces is highly consistent, much more than for other methods. NMI and VI yielded nearly constant values (horizontal bands) for many models of a given c_{max} , whereas Lasso yielded a wide spread. While different permutations of the same information content will look different to Lasso, they will be recognized as similar by NMI and VI; the bands are the result of multiple channels for each model containing the same information at higher values of c_{max} . We have left out the largest values of c_{max} , where the transmitted information is so high that the posteriors effectively shrank to points.

E Appendix: Implementation specifics

All experiments were implemented in TensorFlow and run on a single computer with a 12 GB GeForce RTX 3060 GPU.

We have uploaded code to the following repository: <https://github.com/murphyka/representation-space-info-comparison>. The heart of the codebase is in `utils.py`, containing the Bhattacharyya and the NMI/VI calculations. A full working example on the Fashion-MNIST dataset is included as an iPython notebook, as well as the code to reproduce the ensemble learning experiment (Sec. 4.4).

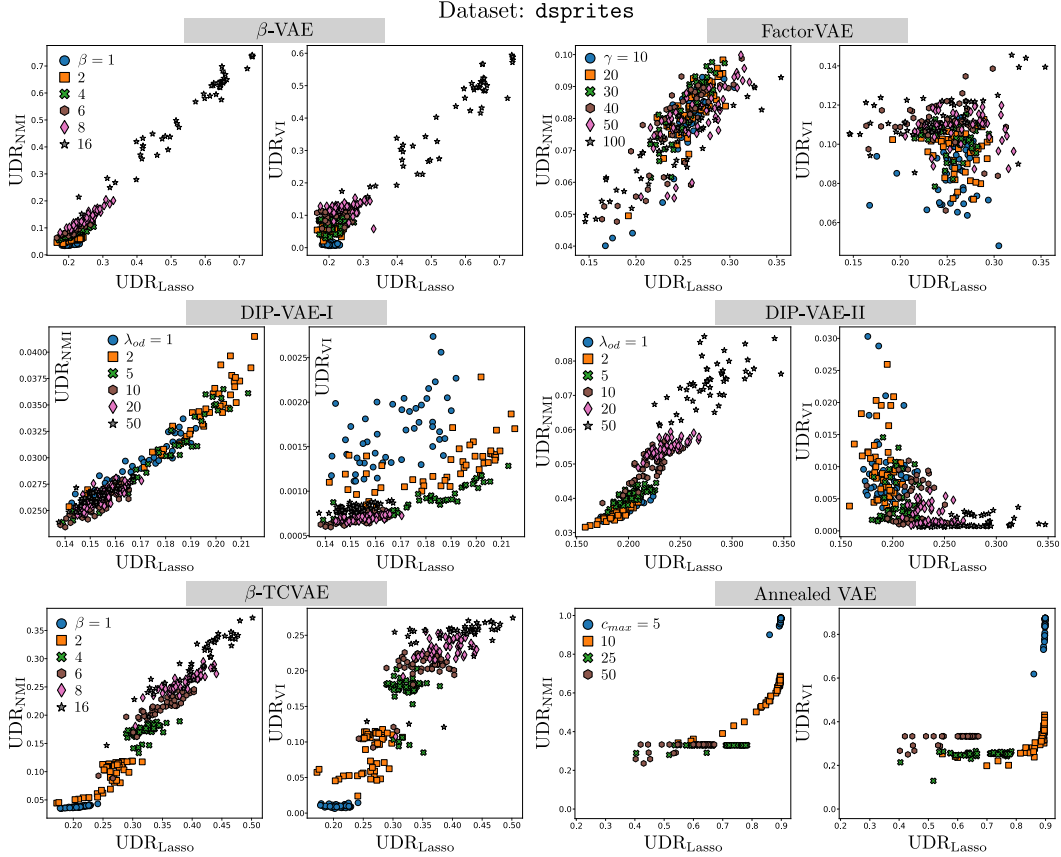


Figure 13: **Extended UDR comparison: dsprites.** We replace the measure of channel similarity in UDR [11] to NMI or $\exp(-VI)$ for multiple sets of models trained by Locatello et al. [1].

Models: For the dsprites, smallnorb, and cars3d datasets, we used the trained models that were publicly released by the authors of Locatello et al. [1]. Thus, all of the model and channel numbers recorded above the latent traversals in Fig. 4h correspond to models that can be downloaded from that paper’s github page³. Simply add the model offset corresponding to the $\beta = 16$ β -VAE for cars3d, 9250 (e.g., for the traversal labelled with model 31 ch 3, download model 9281 and traverse latent dimension 3, 0 indexed).

For the MNIST and Fashion-MNIST ensembles, we trained 50 β -VAEs with a 10-dimensional latent space. The encoder had the following architecture:

```

Conv2D: 32 4×4 ReLU kernels, stride 2, padding ‘same’
Conv2D: 64 4×4 ReLU kernels, stride 2, padding ‘same’
Reshape([-1])
Dense: 256 ReLU
Dense: 20.

```

The decoder had the following architecture:

```

Dense: 7 × 7 × 32 ReLU
Reshape([7, 7, 32])
Conv2DTranspose: 64 4×4 ReLU kernels, stride 2, padding ‘same’
Conv2DTranspose: 32 4×4 ReLU kernels, stride 2, padding ‘same’

```

³https://github.com/google-research/disentanglement_lib/tree/master

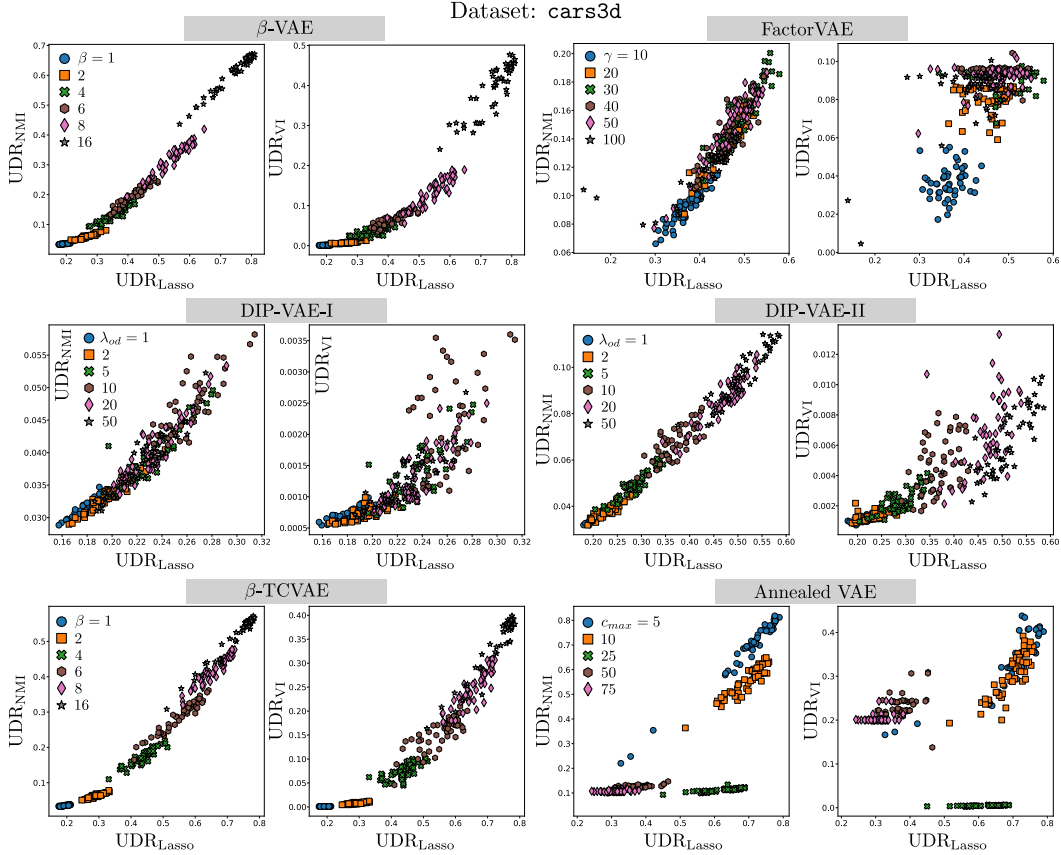


Figure 14: **Extended UDR comparison: cars3d.** We replace the measure of channel similarity in UDR [11] to NMI or $\exp(-VI)$ for multiple sets of models trained by Locatello et al. [1].

Conv2DTranspose: 1 4×4 ReLU kernels, stride 1, padding ‘same’.

The models were trained for 2×10^5 steps, with a Bernoulli loss on the pixels, the Adam optimizer with a learning rate of 10^{-4} , and a batch size of 64.

Clustering analysis: We used the OPTICS implementation from `sklearn`⁴ with ‘precomputed’ distance metric and `min_samples=20` (and all other parameters their default values). For distance matrices we clipped away any negative values in VI and converted NMI to a distance metric with $-\log \max(\text{NMI}, 10^{-4})$.

Ensemble learning: For the ensemble learning toy problem (Sec. 4.4), we trained 250 simple β -VAEs ($\beta=0.03$) whose encoder and decoder were each fully connected networks with two layers of 256 \tanh activation. The input was two-dimensional, the latent space was one-dimensional, and the output was two-dimensional. The loss was MSE, the optimizer was Adam with learning rate 10^{-3} , and the batch size was 2048. Data was sampled anew each batch, uniformly at random from the unit circle.

To perform ensemble learning, we evaluated the Bhattacharyya matrices for 200 evenly spaced points around the unit circle for each model in the ensemble. Then we directly optimized the parameters for 200 posterior distributions (Gaussians with diagonal covariance matrices) in a two-dimensional latent space, so as to maximize the average similarity (NMI or exponentiated negative VI) between the Bhattacharyya matrix for the trainable embeddings and those of the ensemble. We used SGD with a learning rate of 3 for 20,000 iterations, and repeated for 5 trials for each ensemble size.

⁴<https://scikit-learn.org/stable/modules/generated/sklearn.cluster.OPTICS.html>